

# Sensors and Electronic Instrumentation Advances

**Proceedings**

**of the 9<sup>th</sup> International Conference  
on Sensors and Electronic  
Instrumentation Advances  
(SEIA' 2023)**

**20-22 September 2023  
Funchal (Madeira Island), Portugal**



# **Sensors and Electronic Instrumentation Advances:**

**Proceedings of the 9<sup>th</sup> International Conference  
on Sensors and Electronic Instrumentation Advances**

**20-22 September 2023  
Funchal (Madeira Island), Portugal**

**Edited by Sergey Y. Yurish**



Sergey Y. Yurish, *Editor*  
Sensors and Electronic Instrumentation Advances  
SEIA' 2023 Conference Proceedings

Copyright © 2023  
by International Frequency Sensor Association (IFSA) Publishing, S. L.

E-mail (for orders and customer service enquires): [ifsa.books@sensorsportal.com](mailto:ifsa.books@sensorsportal.com)

Visit our Home Page on <http://www.sensorsportal.com>

All rights reserved. This work may not be translated or copied in whole or in part without the written permission of the publisher (IFSA Publishing, S. L., Barcelona, Spain).

Neither the authors nor International Frequency Sensor Association Publishing accept any responsibility or liability for loss or damage occasioned to any person or property through using the material, instructions, methods or ideas contained herein, or acting or refraining from acting as a result of such use.

The use in this publication of trade names, trademarks, service marks, and similar terms, even if they are not identifies as such, is not to be taken as an expression of opinion as to whether or not they are subject to proprietary rights.

ISBN: 978-84-09-53746-4  
BN-20230915-XX  
BIC: TJFC

## Contents

<b>Foreword .....</b>	<b>5</b>
<b>Fiber Optic Current Sensor Based on 22.5° Faraday Rotator and Polarizing Beam Splitter .....</b>	<b>6</b>
<i>A. Madaschi, P. Martelli and P. Boffi</i>	
<b>Detection of Trafficable Areas in Outdoors with a Downward Looking 2D LiDAR .....</b>	<b>9</b>
<i>A. Olivas and F. Torres</i>	
<b>Hardware Acceleration of Pulse Analysis using FPGAs in MicroTCA .....</b>	<b>12</b>
<i>C. Gonzalez, M. Ruiz, A. Carpeño, A. Pinas, D. Cano-Ott, J.Plaza, T. Martinez, D.Villamarin</i>	
<b>Advanced Polymer Materials for Real-time Sensing of Inflammation and Infection.....</b>	<b>16</b>
<i>M. Hrubý, H. Zhukouskaya and E. Tomšik</i>	
<b>Software Defined Radio Based Concept for Extending Orthogonal Multi-tone Time Domain Reflectometry Method to Analyze Electrical Power Grids .....</b>	<b>18</b>
<i>A. Faschingbauer</i>	
<b>Traffic Signaling and Cooperative Trajectories based on Visible Light Communication .....</b>	<b>23</b>
<i>M. A. Vieira, G. Galvão, M. Vieira, M. Véstias P. Vieira, and P. Louro</i>	
<b>Visible Light: An Identifier (ID) System for Building Guidance.....</b>	<b>29</b>
<i>M. Vieira, M. A. Vieira, P. Vieira, and P. Louro</i>	
<b>Classification of Sports Exercises and Repetition Counting based on Inertial Measurement Data .....</b>	<b>35</b>
<i>P. Krutz, M. Rehm, Z. Lang, M. Dix and J. Patalas-Maliszewska</i>	
<b>Difference in Sensor Placement Position of Insole-type Pressure Transducers .....</b>	<b>40</b>
<i>Y. Uchida, T. Funayama, E. Ohkubo and Y. Kogure</i>	
<b>Electrochemical Determination of Cd<sup>2+</sup>, Pb<sup>2+</sup>, Cu<sup>2+</sup> and Zn<sup>2+</sup> in Liquids using Modified Titanium Dioxide.....</b>	<b>44</b>
<i>Vorobets V. S., Fomanyuk S. S., Medyk I. A., Kolbasov G. Ya., Karpenko S. V.</i>	
<b>Near-Field Microwave Probe Technique for Local Broadband Characterization of Nanocomposite Materials.....</b>	<b>48</b>
<i>H. Bakli and M. Makhoulf</i>	
<b>Comparison of the Depth Accuracy of a Plenoptic Camera and a Stereo Camera System in Spatially Tracking Single Refuse-derived Fuel Particles in a Drop Shaft.....</b>	<b>52</b>
<i>M. Zhang, R. Streier, M. Vogelbacher, S. Wirtz, V. Scherer, and J. Matthes</i>	
<b>Impact of Solvent on Ammonia Detection Performance of Polyaniline-based Sensors.....</b>	<b>58</b>
<i>S. Vassaux, N. Redon, E. A. da Silva and C. Duc</i>	
<b>Feasibility of Gait Change Detection using Smart Footwears .....</b>	<b>60</b>
<i>T. Funayama, Y. Uchida, Y. Kogure, D. Souma, R. Kimura</i>	
<b>Exploring the Hidden Complexity: Approximate Entropy and Sample Entropy Analysis in Pulse Oximetry of Female Athletes.....</b>	<b>64</b>
<i>A. M. Cabanas, D. Catalán, N. Sáez, C. Flores, and P. Martín-Escudero</i>	
<b>Development of a Smart Irrigation System for Apple Fields using a LoRaWAN Network.....</b>	<b>70</b>
<i>R. Mendicino, S. Tritini, A. Mejia-Aguilar, and R. Monsorno</i>	
<b>The use of Azure Cloud Tools for Monitoring Indoor Air Quality .....</b>	<b>74</b>
<i>L. C. Eduardo, C.R.S. Alexandre and A. S. F. Tercio</i>	
<b>Visible Light Communication for Indoors Automated Guidance Vehicles .....</b>	<b>76</b>
<i>P. Louro, M. Vieira, M. A. Vieira</i>	
<b>Wind Estimation via UAV Parameters and Artificial Intelligence related to Ultrasonic Anemometer Measurements .....</b>	<b>80</b>
<i>Michael Kurz, Federico Mothes, Markus Kreuzer, Alexander Knoll</i>	
<b>Digital Twin-based Models of Human Activities, Localization, and Energy Consumption of WBAN Network using IMU Sensors.....</b>	<b>83</b>
<i>Noureddine Boujnah, Rafika Brahma and Ridha Ejbali</i>	

<b>Sensing the Mechanical Properties of AlN Thin Films using Micromechanical Membranes.....</b>	<b>90</b>
<i>Aditya, T. Sommer, M. Althammer, and M. Poot</i>	
<b>Video Stream Processing for an Autonomous Tunnel Drainage Rover.....</b>	<b>94</b>
<i>A. L. Giordano, T. Schachinger, V. Micic Batka, and B. G. Zaggar</i>	
<b>An IoT Communication Platform for Interactive Buildings Energy Management System.....</b>	<b>99</b>
<i>L. Mihet-Popa</i>	
<b>Geospatial Sensor-based Approach to Provide Defibrillators by using Drones in Mountain Areas: A Study Case in South Tyrol, Italy .....</b>	<b>104</b>
<i>E. Fajardo-Figueroa, R. Mendicino, S. Tritini, M. van Veelen, G. Vinetti, G. Ristorto, S. Mayrgündter, G. M. Bianco, L. Meng and A. Mejia-Aguilar</i>	
<b>Zinc Tin Oxide Nanostructures Synthesized by the Microwave Hydrothermal Method Applied to Gas Sensors.....</b>	<b>107</b>
<i>R. A. Silva, M. G. Masteghin and M. O. Orlandi</i>	
<b>Replication of a DSC Device Using 3D Computational Modelling: Correction of Heat Flow Diagrams of Selected Geopolymers by Processing the Experimental Data .....</b>	<b>109</b>
<i>V. Kočí</i>	
<b>Exploring Sustainable Printed Paper Sensors for Analyzing Cure Behavior and Detecting Cracks in Composites .....</b>	<b>111</b>
<i>A. Mahendran, N.Gupta, C. Koren and H. Lammer</i>	
<b>Exploration of Phage Display Peptides as Novel Sensing Materials for Highly Sensitive and Selective Biomimetic Optoelectronic Nose .....</b>	<b>114</b>
<i>V. Escobar, C. Hurot, S. Brenet, M. El Kazzy, N. Scaramozzino, R. Mathey, A. Buhot, and Y. Hou</i>	
<b>Calibration of a Hail-Impact Sensor based on Piezoelectric Transducers .....</b>	<b>117</b>
<i>F. Blasina, A. Echarri and N. Pérez</i>	
<b>Terahertz Sensor System with Dual Mode Operation.....</b>	<b>120</b>
<i>Janez Trontelj, Andrej Švigelj, Domen Višnar, Janez Trontelj jr.</i>	
<b>Physiological Assistance by Climate Comfort: Measurements and Indicators.....</b>	<b>124</b>
<i>Bernhard Kurz, Christoph Russ</i>	
<b>Internet of Things-based Geo-awareness System for Civilian Drones.....</b>	<b>128</b>
<i>S. Kunze</i>	
<b>Hyperspectral Imaging Microscopy for Single-cell-analysis.....</b>	<b>133</b>
<i>Wolfgang Kurz, Aaron Flügge Arus, Emre Kariper, Olcay Akgün, Edwin Adisoemarta, Martin Jakobi, Alexander W. Koch</i>	
<b>Development of Bimetallic Zn/Ti-BMOF Thin Film Composite Optical Waveguides for Ethylenediamin Detection at Ambient Temperature .....</b>	<b>136</b>
<i>Patima Nizamidin , Huifang Chen</i>	
<b>Routine Measurement and Monitoring System for the Activity of Elderly People with Dementia: A Systematic Review.....</b>	<b>139</b>
<i>Júlia D. Rodrigues, Pedro Morais and Vítor Carvalho</i>	
<b>Virtual Reality and Artificial Intelligence as Tools to Aid the Management of Chronic Pain: A Comprehensive Literature Review.....</b>	<b>145</b>
<i>Arthur Gomes, Anabela Marques, Vítor Carvalho and Duarte Duque</i>	
<b>Using Machine Learning to Classify Network Abnormalities into Legitimate or Assault in IoT-based Cyber Physical System.....</b>	<b>150</b>
<i>Stephen Afrifa, Vijayakumar Varadarajan, Peter Appiahene and Tao Zhang</i>	
<b>Vehicle Speed Measurement through Ground Vibrations Induced by Transverse Rumble Strips .....</b>	<b>154</b>
<i>D. Thanglerdsumpun, P. Wardkein and L. Kirasamuthranon</i>	
<b>Static and Dynamic Calibration of Pneumatic Pressure Sensors and Instruments.....</b>	<b>160</b>
<i>José Dias Pereira, Octavian Postolache</i>	
<b>APHRODITE: Design and Preliminary Tests of an Autonomous and Reusable Photo-sensing Device for Immunological Test aboard the International Space Station.....</b>	<b>164</b>
<i>L. Nardi, N. Maipan Davis, S. Sansolini, T. B. De Albuquerque, M. Laarraj, D. Caputo, G. de Cesare, S. R. Shariati Pour, M. Zangheri, D. Calabria, M. Guardigli, M. Balsamo, E. Carrubba, F. Carubia, M. Ceccarelli, M. Ghiozzi, L. Popova, A. Tenaglia, M. Crisconio, A. Donati, A. Nascetti, M. Mirasoli</i>	

(020)

# Comparison of the Depth Accuracy of a Plenoptic Camera and a Stereo Camera System in Spatially Tracking Single Refuse-derived Fuel Particles in a Drop Shaft

**M. Zhang**<sup>1</sup>, **R. Streier**<sup>2</sup>, **M. Vogelbacher**<sup>1</sup>, **S. Wirtz**<sup>2</sup>, **V. Scherer**<sup>2</sup> and **J. Matthes**<sup>1</sup>

<sup>1</sup>Karlsruhe Institute of Technology, Institute for Automation and Applied Informatics,  
Hermann-von-Helmholtz-Platz 1, 76344 Eggenstein-Leopoldshafen, Germany

<sup>2</sup>Ruhr-University Bochum, Department of Energy Plant Technology,  
Universitätstr. 150, 44801, Bochum, Germany

Tel.: + 49 721 608-24919, fax: + 49 721 608-22602

E-mail: miao.zhang@kit.edu

---

**Abstract:** With the development of depth cameras in the last decades, several cameras are able to acquire 3D information of the captured scenes, such as plenoptic camera and stereo camera system. Because of the differences in principle and construction of various depth cameras, different cameras own particular advantages and disadvantages. Therefore, a comprehensive and detailed comparison of different cameras is essential to select the right camera for the application. Our research compared the depth accuracy and stability of a stereo camera system and a plenoptic camera by monitoring the settling processes of various refuse-derived fuel particles in a drop shaft. The particles are detected at first using detection approaches, and the particle detections are subsequently associated in accordance with data association algorithms. The spatial particle trajectories are obtained by the tracking-by-detection approach, based on which the performances of the cameras are evaluated.

**Keywords:** 3D Measurement, Plenoptic camera, Stereo camera system, Particle tracking-by-detection, Comparison of 3D sensors.

---

## 1. Introduction

The knowledge of 3D measurements is of significant importance in various applications, for instance, object localization and tracking. To achieve the 3D localization of objects, a 3D sensor is quite essential. With the development of measurement techniques, more and more sensors are able to acquire 3D information concerning captured scenes, such as the time-of-flight (ToF) camera [1], the structured light camera [2], the stereo camera system [3], and the plenoptic camera [4]. Given the multiple potential options for 3D cameras, selecting an appropriate solution based on using the environment is of interest to a range of research communities. For instance, in [5], the consumer depth camera Microsoft Kinect with a novel depth imaging technique is compared to the state-of-the-art continuous wave amplitude modulation ToF cameras by a set of experimental setups for the purpose of evaluating the respective merits and drawbacks of the cameras. Further, Chiu *et al.* [6] compared 3D reconstruction results based on data collected by two different types of depth cameras (ToF and stereoscopic cameras) and commercial 3D scanning systems to determine the selection of the depth camera concerning the applications.

As indicated by the review of the related works, the ToF camera, the structured light camera, and the stereo camera system have been widely researched regarding their availabilities of providing depth information. Notwithstanding, the research on plenoptic cameras based on the plenoptic function is still scarce, so there is insufficient information concerning comparison

with other depth cameras. In addition, since the plenoptic camera has been developed in recent decades, several issues concerning the plenoptic camera remain problematic, *e.g.*, incomplete corresponding data processing techniques and custom imaging hardware [7].

This study contributes to comparing a plenoptic camera and a stereo camera system in spatially tracking single refuse-derived fuel (RDF) particles in a drop shaft. These two camera systems were selected in accordance with use case addressed (experimental setup, depth, resolution, etc.) and are compared primarily in terms of depth accuracy. Moreover, the structured light camera and the ToF camera are basically not adequate for observing small particles (such as RDF particles), and therefore, only the stereo camera system and plenoptic camera are considered. First, the two cameras measure the depth of objects distributed equidistantly in the drop shaft. Subsequently, the motions of four RDF fractions in the drop shaft, *viz.*, wood chips, PE-granule, paper shred, and confetti, are photographed separately. The captured images are then used to derive the 3D trajectory of each RDF particle by image processing techniques according to the tracking-by-detection principle. By comparing the 3D trajectories from the same object, the performances of cameras can be evaluated.

This paper is structured as follows: in section 2, the experimental setup is illustrated. Section 3 briefly demonstrates the applied image processing approaches to detect and track particles. In section 4, the

corresponding results are discussed. Section 5 concludes the paper.

## 2. Experimental Setup

Single RDF particles are transported to the upper part of the drop shaft and then fall through a tube into the drop shaft, as shown in Fig. 1. As a consequence of the extra distance provided by the tube, the particles are accelerated to their terminal velocities before the recording starts. In order to achieve a high contrast of the illuminated particle to the background, the inner wall of the drop shaft is painted black. With 18 LED modules, the lighting system, located at the top inlet of the drop shaft, is able to offer a total luminous flux of 104,400 lm. Furthermore, a drawer with tilted panels is installed at the bottom of the drop shaft, which ensures one particle within a certain capture period. As schematically depicted in Fig. 1, the total distance between the top edge of the drawer and the location of the cameras is 4.8 m. While the plenoptic camera was fixed directly above the drop shaft, the two stereo cameras were mounted on each side above of the drop shaft. Table 1 lists the technical parameters of the utilized stereo camera system and the plenoptic camera.

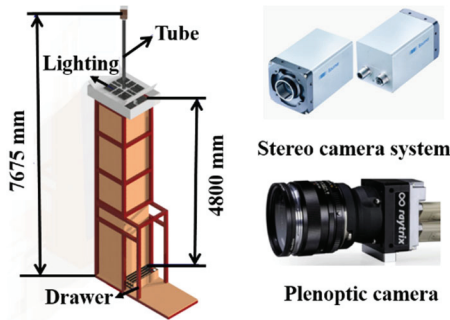


Fig. 1. Schematic of the drop shaft (left) and the utilized two depth camera systems (right).

The stereo camera system was calibrated with a checkerboard in accordance with the calibration method recommended in [8]. Additionally, the intrinsic and extrinsic parameters entailed for the subsequent stereo rectification were also determined. Meanwhile, the plenoptic camera was calibrated based on the principles demonstrated in [9].

Table 1. Technical details of 3D cameras utilized in the study.

	Stereo camera	Plenoptic camera
Manufacturer	Baumer	Raytrix
Model	VLXT-28 M.I	R12
Principles of depth measurement	Stereoscopic camera	Light-field technique
Image resolution	1920 × 1464 px	2048 × 1536 px
Max. frame rate	500 fps	330 fps

RDF contains a broad range of fractions, and four representative fractions, namely wood chips, confetti, paper shreds, and polyethylene (PE) granules, as shown in Figure 2 were selected for the particular experiment. The particles' actual sizes can be roughly estimated according to the 1 cm scale at the bottom right of the figure. Additionally, Table 2 lists the 3D dimensions of the fuel fractions. In the following, the paper presents the comparison of the depth cameras concerning the experiments with the depicted four fractions.



Fig. 2. Various RDF fractions applied in the experiments. (a) Wood chips. (b) Confetti. (c) Paper shreds. (d) PE granules. [10]

Table 2. Physical properties of the experimented RDF fractions

Fraction	Form	Length (mm)	Width (mm)	Thickness (mm)
Wood chips	Cuboid	5-10	4-7	1
Confetti	Round flake	6	6	0.104
Paper shred	Long flake	25-35	6	0.104
PE granule	Round plate	4	4	2

## 3. Image Processing Approaches

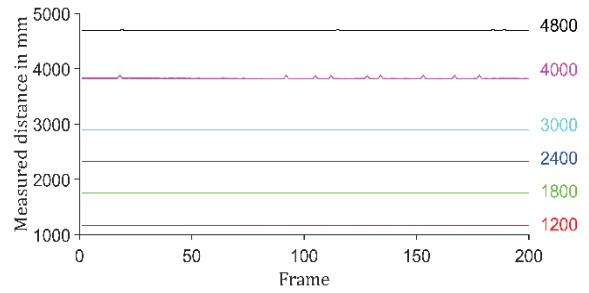
The spatial trajectory of each single RDF particle is derived based on the principle of tracking-by-detection, which identifies objects at first and associates the detections into trajectories afterward. Since the measurements refer to single particle tracking-by-detection, the detection and tracking process are relatively uncomplicated. The particles are identified by virtue of binarization and then associated temporally. The available image processing approaches for multiple particle tracking-by-detection

using the plenoptic camera are presented in [11], which include a novel combined detection method and a data association approach using a linear Kalman filter with the 2.5D global nearest neighbor approach. The same image processing procedure can also be used on the stereo camera system. Notwithstanding, as a consequence of the higher depth accuracy provided by the stereo camera system, the processing might be refined accordingly.

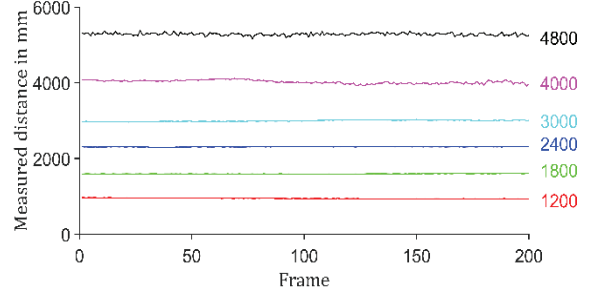
#### 4. Results and Discussion

First, in order to obtain an initial estimate of the accuracy of the two cameras, both cameras measured the distance to a calibration object simultaneously, where the object was placed at six different depth positions. For each captured image, plenty of pixels belonging to the object can be captured. Hereby, we recognize a mean depth as the representing depth of the object. Fig. 3 shows the depths of the calibration object with different ground truth depths measured by both camera systems, where 200 measured depth points of each ground truth depth are selected and displayed in the figure. Additionally, Fig. 4 presents the comparison result by a boxplot to point out the measured median distance and its corresponding distribution over time. The zero point is defined as the upper edge of the drop shaft scaffold, which is 4.8 m to the bottom. As revealed by the figure, the stereo camera system delivers median measured distances smaller than the ground truth values, whereas the plenoptic camera system measures the distances that are first smaller and then larger than the true values. Moreover, the measurement deviation of the stereo camera system tends to increase as the measurement distance increases. Comparatively, the measurement error of the plenoptic camera decreases at first, roughly minimized at around 3 m to 4 m, and then boosts. Compared to 4 m, where the median measurement deviates from the ground truth value by only 48 mm, the error at 4.8 m reaches 470 mm. Overall, the stereo camera shows superior stability and accuracy in measuring the distance of non-moving objects compared to the plenoptic camera.

In addition to comparing the differences between the two depth cameras in measuring fixed calibration objects, the cameras are also compared for measuring continuously varying depths of the calibration object, as schematically depicted in Fig. 5. The varying distance is measured five times, and the resulting five trajectories are shown in the figure. Generally, the distance changes measured by the two cameras are comparable. As revealed in Fig. 5, the measurements of the plenoptic camera are accompanied by more significant fluctuations, especially at the beginning and the end. Since the drop shaft is 4.8 m high, the trajectory should end up fluctuating slightly at 4.8 m. Therefore, we can deduce a larger measured value of the plenoptic camera at 4.8 m, which indicates an agreement with the statement provided in Fig. 4.

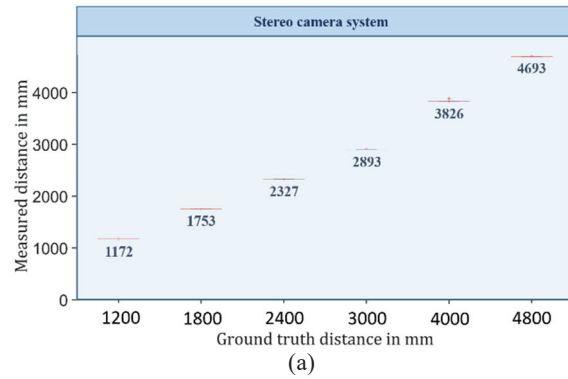


(a) Stereo camera system

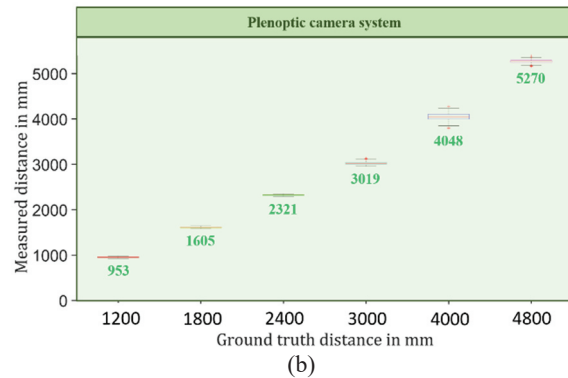


(b) Plenoptic camera system

**Fig. 3.** Measured depth of the calibration object with different ground truth depths. The horizontal coordinate is the frame number, and the vertical coordinate represents the measured distance.



(a)



(b)

**Fig. 4.** Boxplot of measured depth. The horizontal coordinate is the actual distance of the object, and the vertical coordinate represents the measured distance. (a) Measured distance of the stereo camera system. The S refers to the stereo camera, and the blue number is the median of the measured value. (b) Measured distance of the plenoptic camera system. The P stands for the measured value of the plenoptic camera, and the green number is the corresponding temporal median.

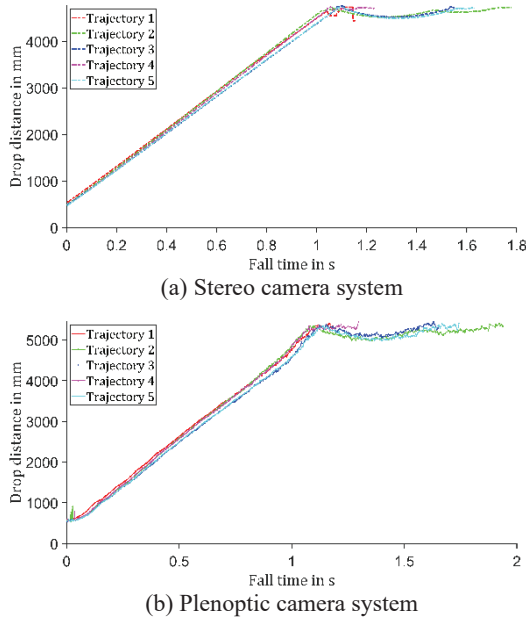


**Fig. 5.** Measured continuously increasing drop distance with relation to fall time. The horizontal coordinate is the fall time, and the vertical coordinate represents the drop distance.

As a result of completing the comparison of measuring the distance of fixed objects and continuously increasing distances, an initial impression of the accuracy of the two cameras is obtained. Thereafter, the trajectories of various RDF particles derived by the two cameras are also compared. For each fraction, ten particles were dropped, detected, and tracked. For clarity, only one trajectory of each fraction is presented in Fig. 6.

Because the two cameras were triggered asynchronously and their captured ranges differed, time differences exist between the captured corresponding trajectories. In order to achieve a visual comparison of the trajectories' similarities, the trajectories captured by the plenoptic camera are delayed by a certain amount of time. For the purpose of determining the time, the average value of the first ten captured depths by the plenoptic camera is computed. Subsequently, the depth value that is closest to the average value on the captured trajectory belonging to the stereo camera system is searched, and the corresponding time is the delay time. Apparently, the plenoptic camera provides a longer measured depth range, especially when tracking smaller particles such as confetti and plastics. As far as stability is concerned, the fluctuations of the trajectories with respect to all fractions provided by the plenoptic camera are much more substantial than those of the stereo camera system, as also revealed in the previous experiments. The measurement fluctuations of the plenoptic camera are more considerable than the stereo camera system for measuring both stationary and moving objects. Moreover, the fluctuations of measuring small objects are even more significant, which is not conducive to object tracking. Although the trajectories provided by the stereo camera system fluctuate more slightly, small

particles can be detected and tracked longer by the plenoptic camera.

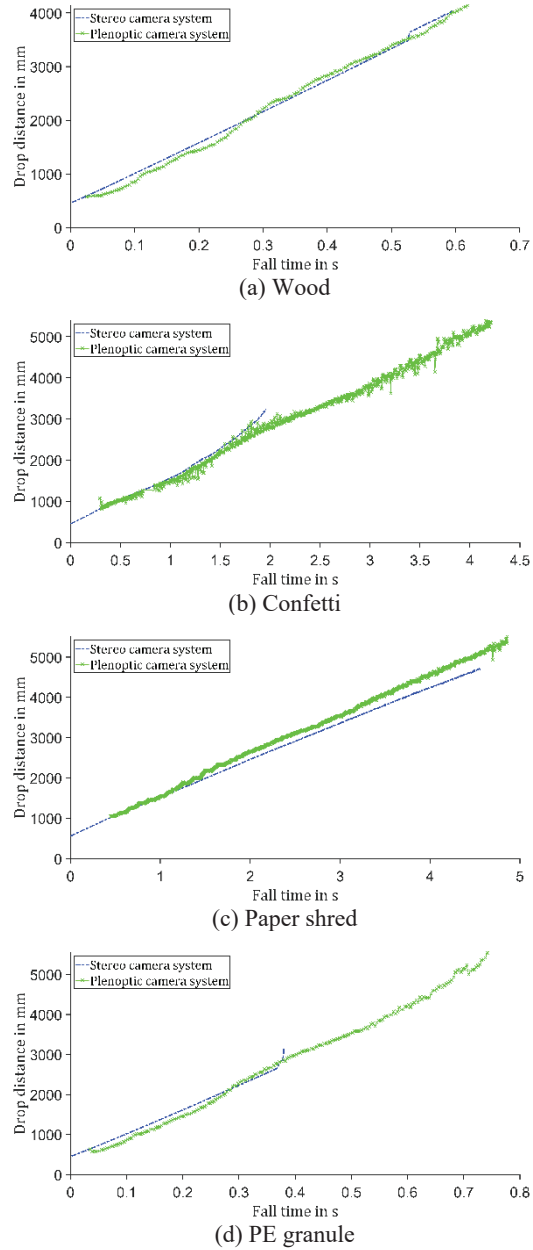


**Fig. 6.** Examples of drop distance with relation to fall time of various particle fractions. The horizontal coordinate is the fall time, and the vertical coordinate represents the drop distance.

In addition, the point-based similarity of the resulting trajectories of each particle is computed according to dynamic time warping [12], which aims to find the warping path between two trajectories with the smallest warping cost. Dynamic time warping can compute the similarity of two time series (*e.g.*, the time-depth trajectory), especially for time series with different lengths and frame rates. Dynamic time warping warps and distorts the time series automatically (*i.e.*, localized scaling on the time axis)

so that the two signals are as consistent as possible to obtain the maximum similarity. Supposing two time series Q and C with respective lengths n and m, the value of the  $i^{\text{th}}$  frame from Q is denoted as  $q_i$  and the value of the  $j^{\text{th}}$  frame from C as  $c_j$  afterward. To align these two series, a matrix of the dimension  $n \times m$  is constructed with matrix elements  $(i, j)$  denoting the Euclidean distance between the two points  $q_i$  and  $c_j$ . The smaller the distance, the higher the similarity. Dynamic time warping finds the minimum of the sum of the Euclidean distances and recognizes the sum as the warping cost. The dynamic time warping takes the time shift into consideration and is thus superior to simply computing the Euclidean distance between the corresponding trajectories. Fig. 7 gives an example of the distance between two trajectories (obtained signals) using dynamic time warping. The figure above depicts the originally measured distances of the two cameras, and the bottom figure presents the comparison of the distances using dynamic time warping. The outcome of the comparison is the sum of the Euclidean distances between corresponding points.

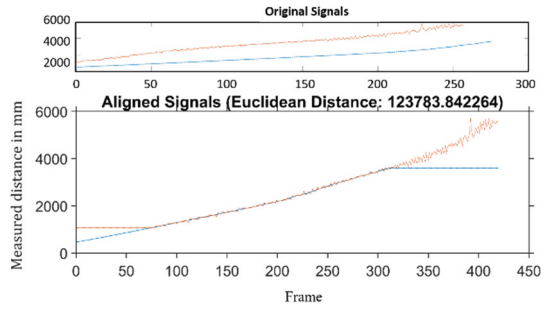


**Fig. 7.** Schematic of the point-based similarity utilizing dynamic time warping. The horizontal coordinate is the captured frame, and the vertical coordinate represents the measured drop distance.

Table 3 illustrates the computed median distances of the fractions in accordance with dynamic time warping. The bottom row of Table 3 indicates the distance normalized by the number of frames. As presented in Fig. 7, the trajectory is automatically patched according to the initial or termination value after the shifting to ensure the same length, which gives rise to more considerable distances. Therefore, the larger the time difference between the two trajectories, the further the resulting distance will be. As shown in Table 3, wood chip has shorter matching distance as a consequence of its regular and rapid movement. Compared to wood chip, confetti and paper shred have a larger windward area and greater wind resistance. As a result, their falling motions tend to be more irregular and slower, leading to longer trajectory distances. This can also be indicated by the trajectory instances in Fig. 6. Although PE also triggers regular movement, the difference existing in the captured range of the two cameras results in a large standardized warping distance.

**Table 3.** Median distances of the fractions in mm using dynamic time warping.

Fraction	Wood chips	Confetti	Paper shred	PE granule
Distance	101212	420171	644593	159781
Standardized distance	241.55	325.32	323.21	491.20

## 5. Conclusions

The study compared two different 3D cameras, *viz.*, a stereo camera system and a plenoptic camera, preliminarily with respect to their depth accuracy and stability in measuring the depth of fixed calibration objects, continuously varying depths, and tracking various single RDF fractions in a drop shaft. Concerning measuring the depth of fixed objects, the two cameras are able to provide comparable depth accuracy. The accuracy of the stereo camera decreases with increasing distance, whereas the measurement deviation of the plenoptic camera is nonlinear, which decreases at first and then rises. Additionally, the plenoptic camera measures the depth with the presence of a considerable variation, which shows a negative impact on the tracking process. The same statement can also be deduced when measuring the continuously varying depths. Generally, the two cameras deliver falling distances with a high agreement between each other. Nevertheless, the depth stability provided by the stereo camera is superior. When comparing the cameras in tracking fuel particles, the point-based matching distance using dynamic time warping is introduced to illustrate the similarity between the measured depth trajectories. The distances of the fractions with regular and rapid motions, *e.g.*, wood chips and PE granules, are significantly shorter than those with long-time motions. Furthermore, with the plenoptic camera, the small particles are longer visible. Hence, we can infer a longer observation of the small particles with the plenoptic camera.

To conclude, the stereo camera system and the plenoptic camera could provide comparable depth accuracy. In this regard, the stereo camera system shows a slight advantage. However, the measurement stability of the stereo camera system is far superior to the plenoptic camera. Since the measured depth of the plenoptic camera is accompanied by considerable fluctuations, their impacts on further tracking processes can not be ignored. In several cases, more sophisticated tracking approaches or post-processing are essential to deal with the depth fluctuations caused by the plenoptic camera. On condition that the issues caused by fluctuations can be tackled, the plenoptic camera can replace the stereo camera system in situations, where the stereo camera system can not be applied, such as only one opening is available.

## Acknowledgements

This study is supported by AiF-German Federation of Industrial Research Associations (No. 20410N).